Highly uniform holographic microtrap arrays for single atom trapping using a feedback optimization of in-trap fluorescence measurements

Hikaru Tamura,[1,*] Tomoyuki Unakami,[1] Jun He,[2] Yoko Miyamoto,[3] and Ken'ichi Nakagawa[1]

[1]*Institute for Laser Science, University of Electro-Communications, 1-5-1 Chofugaoka, Chofu 182-8585, Japan*

[2]*State Key Laboratory of Quantum Optics and Quantum Optics Devices, and Institute of OptoElectronics, Shanxi University, Taiyuan 030006, China*

[3]*Department of Engineering Science, University of Electro-Communications, 1-5-1, Chofugaoka, Chofu, Tokyo 182-8585, Japan*

[*]*h_tamura@ils.uec.ac.jp*

Abstract: We report on the novel optimization method to realize highly uniform microtrap arrays for single atom trapping with a spatial light modulator (SLM). This method consists of two iterative feedback loops with the measurements of both diffracted light intensities and in-trap fluorescence intensities from each microtrap. By applying this method to the single ^{87}Rb atom trapping, we can reduce the variance of trap depths from 20.8 % to 1.7 % for 4×4 square arrays and less than 4 % for various arrays with up to 62 sites. The detection error of individual single atoms is also reduced from 1.7 % to 0.0054 % on average.

OCIS codes: (020.3320) Laser cooling; (020.7010) Laser trapping; (270.5585) Quantum information and processing; (090.2890) Holographic optical elements.

References and links

1. D. Meschede and A. Rauschenbeutel, "Manipulating single atoms," Adv. At. Mol. Opt. Phys. **53**, 75–104 (2006).
2. M. Saffman, T. Walker, and K. Mølmer, "Quantum information with Rydberg atoms," Rev. Mod. Phys. **82**, 2313 (2010).
3. I. Bloch, J. Dalibard, and W. Zwerger, "Many-body physics with ultracold gases," Rev. Mod. Phys. **80**, 885 (2008).
4. I. Bloch, J. Dalibard, and S. Nascimbène, "Quantum simulations with ultracold quantum gases," Nat. Phys. **8**, 267–276 (2012).
5. A. M. Kaufman, B. J. Lester, C. M. Reynolds, M. L. Wall, M. Foss-Feig, K. R. A. Hazzard, A. M. Rey, and C. A. Regal, "Two-particle quantum interference in tunnel-coupled optical tweezers," Science **345**, 306–309 (2014).
6. A. M. Kaufman, B. J. Lester, M. Foss-Feig, M. L. Wall, A. M. Rey, and C. A. Regal, "Entangling two transportable neutral atoms via local spin exchange," Nature **527**, 208–211 (2015).
7. T. Wilk, A. Gaëtan, C. Evellin, J. Wolters, Y. Miroshnychenko, P. Grangier, and A. Browaeys, "Entanglement of two individual neutral atoms using Rydberg blockade," Phys. Rev. Lett. **104**, 010502 (2010).
8. L. Isenhower, E. Urban, X. L. Zhang, A. T. Gill, T. Henage, T. A. Johnson, T. G. Walker, and M. Saffman, "Demonstration of a neutral atom controlled-NOT quantum gate," Phys. Rev. Lett. **104**, 010503 (2010).
9. D. Barredo, H. Labuhn, S. Ravets, T. Lahaye, A. Browaeys, and C. S. Adams, "Coherent excitation transfer in a spin chain of three Rydberg atoms," Phys. Rev. Lett. **114**, 113002 (2015).
10. B. J. Lester, N. Luick, A. M. Kaufman, C. M. Reynolds, and C. A. Regal, "Rapid production of uniformly filled arrays of neutral atoms," Phys. Rev. Lett. **115**, 073003 (2015).

#259744 Received 25 Feb 2016; revised 30 Mar 2016; accepted 30 Mar 2016; published 6 Apr 2016

11. S. Bergamini, B. Darquié, M. Jones, L. Jacubowiez, A. Browaeys, and P. Grangier, "Holographic generation of microtrap arrays for single atoms by use of a programmable phase modulator," J. Opt. Soc. Am. B **21**, 1889–1894 (2004).
12. S. Yu, X. He, P. Xu, M. Liu, J. Wang, and M. Zhan, "Single atoms in the ring lattice for quantum information processing and quantum simulation," Chin. Sci. Bull. **57**, 1931–1945 (2012).
13. F. Nogrette, H. Labuhn, S. Ravets, D. Barredo, L. Béguin, A. Vernier, T. Lahaye, and A. Browaeys, "Single-atom trapping in holographic 2D arrays of microtraps with arbitrary geometries," Phys. Rev. X **4**, 021034 (2014).
14. R. W. Gerchberg and W. O. Saxton, "A practical algorithm for the determination of phase from image and diffraction plane pictures," Optik **35**, 237–246 (1972).
15. J. E. Curtis, B. A. Koss, and D. G. Grier, "Dynamic holographic optical tweezers," Opt. Commun. **207**, 169–175 (2002).
16. M. Pasienski and B. DeMarco, "A high-accuracy algorithm for designing arbitrary holographic atom traps," Opt. Express **16**, 2176–2190 (2008).
17. R. Di Leonardo, "Computer generation of optimal holograms for optical trap arrays," Opt. Express **15**, 1913–1922 (2007).
18. G. D. Bruce, M. Y. H. Johnson, E. Cormack, D. A. W. Richards, J. Mayoh, and D. Cassettari, "Feedback-enhanced algorithm for aberration correction of holographic atom traps," J. Phys. B: At. Mol. Opt. Phys. **48**, 115303 (2015).
19. C. L. Quesada, J. Andilla, and E. M. Badosa, "Correction of aberration in holographic optical tweezers using a ShackHartmann sensor," Appl. Opt. **48**, 1084–1090 (2009).
20. N. Schlosser, G. Reymond, and P. Grangier, "Collisional blockade in microscopic optical dipole traps," Phys. Rev. Lett. **89**, 023005 (2002).
21. Y. H. Fung and M. F. Andersen, "Efficient collisional blockade loading of a single atom into a tight microtrap," New J. Phys. **17**, 073011 (2015).
22. K. D. Nelson, X. Li, and D. S. Weiss, "Imaging single atoms in a three-dimensional array," Nat. Phys. **3**, 556–560 (2007).
23. M. J. Piotrowicz, M. Lichtman, K. Maller, G. Li, S. Zhang, L. Isenhower, and M. Saffman, "Two-dimensional lattice of blue-detuned atom traps using a projected Gaussian beam array," Phys. Rev. A **88**, 013420 (2013).
24. C. Y. Shih and M. S. Chapma, "Nondestructive light-shift measurements of single atoms in optical dipole traps," Phys. Rev. A **87**, 063408 (2013).

1. Introduction

Single neutral atoms trapped in optical microtraps are an attractive platform for implementing multi-qubit quantum information processing [1, 2] and studying quantum many-body physics [3–6]. Their weak interactions in the ground state lead to long coherence time and also provide an ideal isolated system. The individual atoms with a moderately large spacing can be strongly correlated via long-range interactions between highly excited Rydberg atoms [7–9]. However, it is a challenge how to scale up this bottom-up approach to a large scale quantum system. The arrays of microtraps with high degree of freedom can be now generated using techniques including acousto-optic deflection [10] and phase-modulation [11–13] of trapping light. The required conditions for their implementation are realizing arrays with a single atom per site and also detecting individual atoms in each trap with high fidelity. A common technique for the site-resolved detection is sub-Doppler cooling by using a homogeneous red-detuned light. However, poor uniformity of trap depths in arrays increases the detection error due to the variance of cooling efficiency and the photon scattering rate from each atom.

The advantage of using the holographic method to generate trap arrays is that holograms corresponding to various trap geometries can be designed, calculated and reconfigured with a spatial light modulator (SLM), which can be placed in the Fourier plane of an optical system. In particular, complex geometries, e.g. triangle, honeycomb or kagome arrays with single atoms are interesting tools for simulating of spin Hamiltonians. To obtain desired arrays of microtraps, iterative Fourier transform algorithms are used for calculating holograms. The original one is the Gerchberg-Saxton (GS) algorithm [14], which has higher diffraction efficiency compared with the other methods such as Generalized Adaptive-Additive method [15] or Mixed-Region Amplitude Freedom (MRAF) algorithm [16]. The high efficiency is necessary to create multi-traps with a mK range of trap depths for precooled atoms with temperature of a few tens of μK

#259744 Received 25 Feb 2016; revised 30 Mar 2016; accepted 30 Mar 2016; published 6 Apr 2016

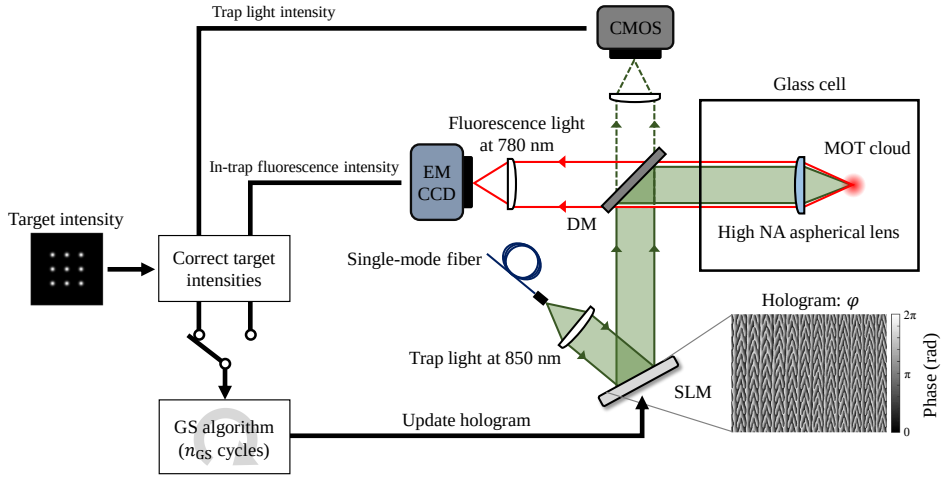

Fig. 1. Schematic of the experimental setup and block diagram of the optimization process. The trap light at a wavelength of 850 nm is reflected by the SLM that can modulate the phase of the light with the calculated pattern. The light transmitted through a dichroic mirror (DM) is measured with a CMOS camera. The trap light is strongly focused onto a MOT region by an aspherical lens operating under the ultrahigh vacuum glass cell. The lens is also used to collect the fluorescence at 780 nm of single atoms. The fluorescence is separated from the trap light by the DM and detected with an EMCCD camera. We correct the target intensity of the Gerchberg-Saxton (GS) algorithm by taking the trap light intensities and the in-trap fluorescence intensities. We then use the corrected target intensity as the input for the GS algorithm, which generates a new hologram for the next iteration.

range. In a practical optical system, results of the calculated holograms are not uniform due to real optics and devices. For the optimization of the uniformity of trap depths, iterative feedback methods have demonstrated in [13,17,18] by using the measured light intensities. However, the actual trap depths for atoms are slightly different from the measured light intensities due to the different optics between the light intensity measurement and the actual trap.

In this paper, we demonstrate the trap depth optimization of holographic arrays using iterative feedback methods with the measurements not only of trap light intensities but also of in-trap fluorescence intensities of individual atoms. By applying this method to the single ^{87}Rb atom trapping, we can reduce the variance of trap depths to 1.7 % for 4×4 square arrays and less than 4 % for all various arrays with up to 62 sites. The improvements lead to a reduction of the detection error of individual atoms from 1.7 % to 0.0054 % on average.

This article consists as follows. After description of our experimental setup for single atom trapping in holographic arrays, we present a feedback optimization based on trap light intensities. We then show how we further optimize the trap depths by monitoring in-trap fluorescence intensities. We probe the ability of these methods by applying it to interesting patterns of microtraps.

2. Experimental setup

Figure 1 shows our setup for the production of red-detuned optical microtraps where single ^{87}Rb atoms will be trapped in intensity maxima. A trap light at a wavelength of 850 nm, delivered from a single-mode polarization maintaining fiber, illuminates the active area of a SLM (Hamamatsu, X10467-02). The 600×795 pixels can imprint an 8-bit phase pattern on the light. The light is reflected by a dichroic mirror (DM) and focused to a waist $w_0 \simeq 1.0\,\mu$m with a high

#259744 Received 25 Feb 2016; revised 30 Mar 2016; accepted 30 Mar 2016; published 6 Apr 2016

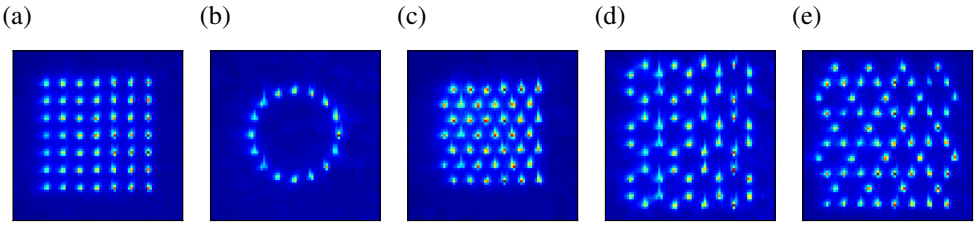

Fig. 2. Averaged fluorescence images of single atoms trapped in (a) square, (b) ring, (c) triangle, (d) honeycomb, and (e) kagome arrays. The images of $60 \times 60\,\mu\mathrm{m}^2$ (each pixel corresponds $0.85 \times 0.85\,\mu\mathrm{m}^2$) are recorded by the EMCCD.

numerical aperture aspherical lens ($NA = 0.5$, $f_{\mathrm{lens}} = 8\,\mathrm{mm}$). A small fraction of the trap light is transmitted through the DM and it is focused on a cooled CMOS camera to monitor the diffracted intensity pattern of the SLM. In order to reduce the thermal drifts of phase modulation levels, the SLM is temperature stabilized and enclosed in a quasi-isolated acrylic box for protecting from air currents.

In our loading procedure, we start with a loading of single atoms by overlapping 1 mK-deep microtraps with a standard magneto-optical trap (MOT), which is loaded from a background rubidium vapor in an ultrahigh vacuum glass cell. The atoms is cooled to $\sim 20\,\mu\mathrm{K}$ with 20 ms of polarization-gradient cooling (PGC). Trapped atoms are detected by fluorescence imaging onto a cooled electron-multiplying CCD (EMCCD) camera with an imaging light. The imaging light contains two laser beams, one is red-detuned by 8 MHz from the free-space D2 $F = 2 \rightarrow F' = 3$ transition and the other is near resonant with the free-space D2 $F = 1 \rightarrow F' = 2$ transition. Each beam is retro-reflected in a one-dimensional lin $\perp$ lin configuration with a Gaussian beam radius of 1.3 mm, which provides sisyphus cooling by exhibiting a polarization gradient. The imaging light is propagating along the trapping plane, where the variance of the imaging light intensity over maximal system size of $60 \times 60\,\mu\mathrm{m}^2$ is smaller than 0.1 %.

Figure 2 represents fluorescence images of single atoms trapped in various two-dimensional arrays that we have created and optimized using the iterative feedback methods with the measurements of both diffracted trap intensities and also in-trap fluorescence intensities. Since each image is an average of 1,000 loading shots with 50 ms exposure time, the brightness of sites depends on loading probability and fluorescence intensity. The spacing between the nearest trap in these arrays is $d \simeq 5\,\mu\mathrm{m}$. We can reduce the spacing d to about $3.6\,\mu\mathrm{m}$ which is limited by the interference between neighboring beams. We can realize about 60 microtrap arrays at maximum which is limited by the available trapping laser power of about 250 mW in our present experimental setup.

3. Feedback optimization of trap depths with light intensity measurement

We first use the standard GS algorithm to generate the holograms for arrays of microtraps such as square, triangle, ring, honeycomb and kagome configurations. The algorithm is initialized with an optical field in the SLM plane created by combining the incident beam profile with a random phase distribution, and the target intensity I_{t} in the trapping plane set to a uniform value for all trap sites. After typically a few ten cycles, the algorithm converges. The calculated hologram is combined with two phase patterns. One is a blazed grating pattern ($2.5\,\mathrm{lp/mm}$) which allows us to separate the traps from the non-diffracted light. The other is a correction pattern in order to compensate the optical flatness defect of the device. The resulting hologram is applied to the SLM. Figure 3(a) shows the intensity distribution of a 10×10 array with $d \simeq 3.6\,\mu\mathrm{m}$ after a single use of the GS algorithm. The area of the image corresponds to $60 \times 60\,\mu\mathrm{m}^2$

#259744 Received 25 Feb 2016; revised 30 Mar 2016; accepted 30 Mar 2016; published 6 Apr 2016

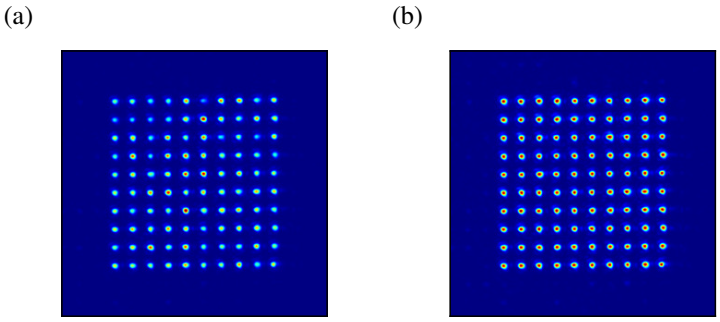

Fig. 3. Trap intensity distributions of a 10×10 square array. The area of the images corresponds to $60 \times 60\,\mu\mathrm{m}^2$ in the actual trapping plane. The images are taken by the CMOS camera (a) before and (b) after 20 iterations of the feedback optimization.

in the actual trapping plane. The trap intensities typically have a dispersion from the average intensity of all sites. If the variance is left uncompensated, some of the sites cannot be loaded with single atoms, because atoms with temperatures higher than 10 % of the trap depth will quickly escape from the trap.

We then implement the feedback optimization method similar to that used in previous similar work [17]. The target image of arrays is adapted individually at each iteration of the process. For the $(i+1)$st iteration, the corrected target intensity of nth site is obtained from

$$I_{\mathrm{t},n}^{(i+1)} = a_n^{(i)} I_{\mathrm{t},n} \tag{1}$$

$$a_n^{(i)} = a_n^{(i-1)} \frac{\langle I_n^{(i)} \rangle}{I_n^{(i)}}, \tag{2}$$

where $I_{\mathrm{t},n}$ and $I_n^{(i)}$ are the target and measurement intensities of the nth site, and $\langle I_n^{(i)} \rangle$ is the average intensity of all sites. The ratio $\langle I_n^{(i)} \rangle / I_n^{(i)}$ represents the weight for the intensity at the nth trap and serves as part of the correction factor $a_n^{(i)}$ for the next iteration in order to reduce deviations in $I_n^{(i)}$ from the average $\langle I_n^{(i)} \rangle$. To improve convergence, $a_n^{(i)}$ includes the previous value $a_n^{(i-1)}$, with $a_n^{(0)}$ set to 1. The output hologram $\varphi^{(i+1)}$ of the GS algorithm, with the previous hologram $\varphi^{(i)}$ as the initial phase pattern and $I_{\mathrm{t},n}^{(i+1)}$ as the corrected target intensity, gives the phase pattern for the next iteration. Compared with previous work [17], we evaluate each intensity $I_n^{(i)}$ from the two-dimensional Gaussian fit to the intensity profile of the image recorded by the CMOS camera, instead of simple integration of the light intensity of each trap. As the beam waist size is slightly different at each trap, two-dimensional Gaussian fits give more accurate determination of the light intensity $I_n^{(i)}$. In comparison with another similar method recently demonstrated in [13], one used in this paper can easily reduce the variance of light intensities without tuning a gain parameter. We evaluate the trap homogeneity by calculating the variance of individual light intensities, which is given by

$$\sigma_{\mathrm{int}} = \frac{1}{\langle I_n \rangle} \sqrt{\frac{1}{N} \sum_{n=1}^{N} |I_n - \langle I_n \rangle|^2}, \tag{3}$$

where N represents the number of traps. In addition, the diffraction efficiency η has been evaluated for each pattern. The efficiency η is defined as a sum of the trap powers P_n divided by the power of the non-diffracted light P_{non} reflected by a uniform phase pattern displayed on

#259744 Received 25 Feb 2016; revised 30 Mar 2016; accepted 30 Mar 2016; published 6 Apr 2016

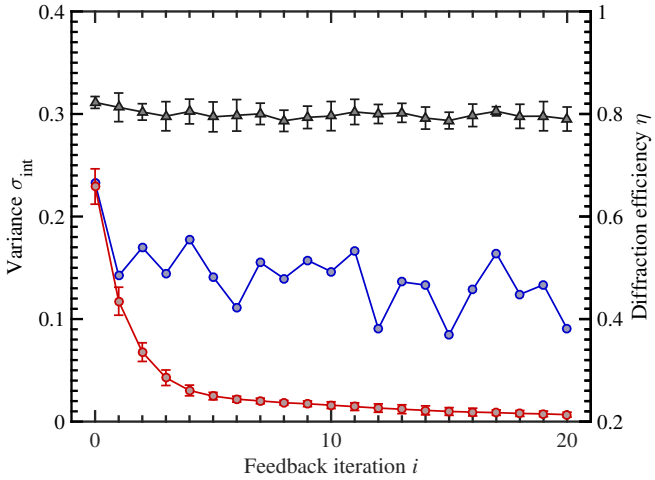

Fig. 4. Performances of the feedback process for 10×10 square arrays. The red circles (black triangles) represent the intensity variance $\sigma_{\rm int}$ (diffraction efficiency η) as a function of feedback iteration i with $n_{\rm GS} = 1$ The error bars are statistical from a sample of five experiments with different initial random phases. The blue circles show $\sigma_{\rm int}$ obtained from a single experiment, where we run the GS algorithm until it converges ($n_{\rm GS} \simeq 40$) for each i-th iteration.

the SLM. We obtain experimental values for P_n by integrating the values of pixels inside a $3.12 \times 3.12\,\mu{\rm m}^2$ square area centered on the peak position.

$\sigma_{\rm int}$ and η recorded at each step of the feedback process for 10×10 square arrays are shown in Fig. 4. We found that the variance of trap intensities can rapidly decrease by reducing the number of cycles of the GS algorithm, denoted as $n_{\rm GS}$, at each feedback step. If we operate the GS algorithm until it converges ($n_{\rm GS} \simeq 40$) at each step, the feedback loop is unable to reduce the intensity variance to below 10 % of the average intensity (blue circles). The oscillation of $\sigma_{\rm int}$ arises from positive or negative correlations of the intensity levels between the neighboring sites. Therefore, we implement the feedback with $n_{\rm GS} = 1$ in order to suppress this oscillation (red circles). The feedback process can dramatically decrease $\sigma_{\rm int}$ during a few initial steps and the remaining steps reduce the residual error step by step. After 20 iterations, $\sigma_{\rm int}$ decreases from 22.9 ± 1.7 % to 0.7 ± 0.2 %. The resulting image of the intensity distribution is shown in Fig. 3(b). The final value of η is 79.0 ± 2.3 %, which is slightly lower than the initial value 82.3 ± 1.2 % due to some of the light going out of the arrays or into intermediate positions between the sites. This decrease depends on the geometry.

We summarize the results after 20 iterations of the feedback algorithm for various arrays, along with N, $\sigma_{\rm int}$, and η in Table 1. Our method can decrease $\sigma_{\rm int}$ to less than 1 % for most patterns. η is typically a few percent lower than the output of a single use of the GS algorithm. Feedback-enhanced algorithm for aberration correction using MRAF algorithm has recently demonstrated in [18]. This method can optimize discrete and also continuous geometries. Compared to this work, our diffraction efficiency is 5.3 times higher for the 10×10 square array and 4.0 times higher for the 16-sites ring array. Currently our method does not correct aberrations but it should be possible to incorporate wave-front optimization with a Shack-Hartmann sensor [13, 19].

#259744 Received 25 Feb 2016; revised 30 Mar 2016; accepted 30 Mar 2016; published 6 Apr 2016

Table 1. Summary of the results after 20 feedback iterations, including number of traps N, variance of the light intensities σ_{int}, and diffraction efficiency η. Each σ_{int} and η is average of five experiments started with different initial phases. Values in round brackets indicate the standard deviation.

		σ_{int} (%)		η (%)	
Structure	N	Before	After	Before	After
4×4 square	16	11.6(1.6)	0.6(0.2)	81.0(1.2)	80.1(1.4)
10×10 square	100	22.9(1.7)	0.7(0.2)	82.3(1.2)	79.0(2.3)
Triangle	72	22.2(2.1)	0.6(0.2)	81.2(2.2)	80.2(1.5)
Ring	16	5.8(2.3)	0.2(0.0)	69.1(0.7)	69.7(0.3)
Honeycomb	54	15.8(0.7)	0.5(0.1)	76.6(1.8)	76.1(1.8)
Kagome	67	21.0(1.1)	0.6(0.1)	78.1(1.5)	76.8(2.3)

4. Feedback optimization of trap depths with in-trap fluorescence measurement

The optimization method described in the last section allows us to realize uniform diffracted intensity pattern which is monitored by the CMOS camera. However, the actual trap depths for atoms are slightly different from the measured light intensities due to the different optics between the light intensity measurement and the actual trap. We found that the variance of trap depths is detrimental for detecting individual atoms with high fidelity. Here, we implement further optimization method by taking in-trap fluorescence intensities from each single atom. Assuming two-level atoms, in-trap fluorescence intensity f_n of nth site during the exposure time $\Delta\tau$ with the total detection efficiency ζ can be written by

$$f_n = \zeta\frac{\Gamma}{2}\frac{s_0}{1+s_0+4(\delta+\Delta_n)^2/\Gamma^2}\Delta\tau, \tag{4}$$

where Δ_n is the total light shift of nth site, Γ is the natural linewidth of D2 line, and $s_0 = I/I_{\text{sat}}$ is the ratio of the imaging light intensity to the saturation intensity. The total light shift Δ_n is directly proportional to the trap light intensity I_n of nth site. Our imaging parameters are detuning of $\delta/2\pi = 8\,\text{MHz}$ from the free space D2 $F = 2 \rightarrow F' = 3$ transition with $s_0 \simeq 3$, and $\Delta\tau = 50\,\text{ms}$. Taking into account $\zeta \simeq 2.2\,\%$ of our optical system and the averaged light shift $\langle\Delta_n\rangle/2\pi \simeq 23\,\text{MHz}$, the number of collected photons per single atom is estimated by 570.

Figure 5(a) shows an averaged fluorescence image of single atoms trapped in a 4×4 square array with spacing $d \simeq 5\,\mu\text{m}$ after the optimization with the intensity measurement. The variance of light intensities measured by the CMOS camera is 0.6 %. For each image, we integrate the nth site signal over the corresponding 5×5 pixels which includes all of the atomic signal without counting the signal from atoms in other sites. The histograms of the integrated signal at each site are shown in Fig. 5(c). These histograms indicate no evidence of doubly occupied sites due to the rapid light-assisted collisions of atomic pair [20]. Therefore, the data on the right (red bars) corresponds to single atom signal and the data on the left (blue bars) is background signal, where the solid black lines are Gaussian fits to the two distributions. We define the in-trap fluorescence intensity f_n as a difference between two peaks of the two distributions in the histogram on nth site.

In order to detect the presence or absence of a single atom with high fidelity, the two distributions should be clearly separated. However, if the trap depth is too high, the in-trap fluorescence intensity decreases due to the large light shift, and leads to the increase of the error in the atom

#259744 Received 25 Feb 2016; revised 30 Mar 2016; accepted 30 Mar 2016; published 6 Apr 2016

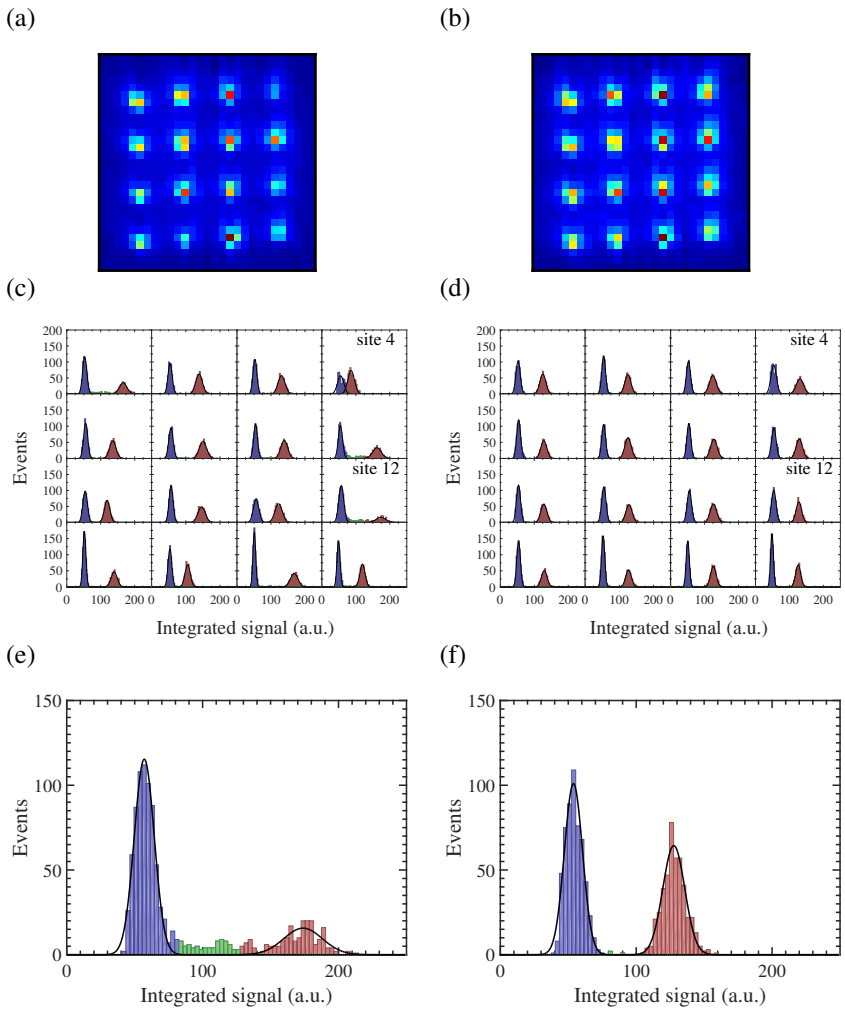

Fig. 5. Single atom trapping in a 4×4 square array and effect of the feedback optimization of in-trap fluorescence intensities. An average of 1,000 fluorescence images (a) before and (b) after five iterations of the feedback algorithm. The images cover an area of $25 \times 25\,\mu\mathrm{m}^2$ (each pixel corresponds $0.85 \times 0.85\,\mu\mathrm{m}^2$) and are recorded by the EMCCD with 50 ms exposure time. (c) Fluorescence detection histograms in each site of the array after optimization using only the trapping light intensity. The red (blue) bars represent the one-atom (zero-atom) signals. The black solid lines are Gaussian fits to the each distribution. (d) Same as in (c), but after the feedback optimization with in-trap fluorescence. The histogram of the integrated signals on site 12 (e) before and (f) after the optimization. The green bars indicate loss counts during the exposure.

detection because the signal distributions for zero and single atom become overlapped [see site 4 in Fig. 5(c)]. By calculating the overlap integration of the two normalized Gaussian distributions, the detection error ε is estimated to be 5.2 % for site 4. On the other hand, if the trap depth is too low, the in-trap fluorescence intensity increases due to the smaller light shift, which leads to the increase of the temperature of atoms in the trap and subsequently a possibility for trap loss during the 50 ms exposure time. Figure 5(e) shows the enlarged histogram for site 12. The data occupying an intermediate position between the two distributions (green bars) can be inferred as a heating loss count during the exposure time. The maximal loss probability of 8.0 %

#259744 Received 25 Feb 2016; revised 30 Mar 2016; accepted 30 Mar 2016; published 6 Apr 2016

Table 2. Summary of the results after i iterations of the in-trap fluorescence feedback, including number of traps N, variance of in-trap fluorescence intensities σ_{fluo}, estimated variance of trap depths σ_{trap}, and maximal detection error ε.

		σ_{fluo} (%)		σ_{trap} (%)		ε		
Structure	N	Before	After	Before	After	Before	After	i
4×4 square	16	28.4	2.4	20.8	1.7	5.2×10^{-2}	2.0×10^{-5}	5
7×7 square	49	16.3	4.0	11.5	2.8	6.0×10^{-3}	4.2×10^{-5}	10
Triangle	42	13.0	5.7	9.1	4.0	2.1×10^{-2}	2.6×10^{-5}	8
Ring	16	24.6	2.7	17.8	1.9	2.6×10^{-3}	8.1×10^{-5}	3
Honeycomb	54	14.8	4.6	10.4	3.2	1.3×10^{-2}	8.4×10^{-5}	9
Kagome	62	18.0	5.8	12.8	4.0	9.6×10^{-3}	7.1×10^{-5}	8

appears on this site. Another loss is caused by background gas collisions, which evenly occurs at all sites with less than 0.5 % probability.

To reduce the variance of trap depths, we implement a similar feedback method to that described in the previous section. The difference is that the individual target intensities of the GS algorithm are determined from in-trap fluorescence intensities of single atoms. At ith iteration, we calculate the target intensity by using Eqs. (1) and (2), where the actual light intensity $I_n^{(i)}$ and the averaged intensity $\langle I_n^{(i)}\rangle$ are estimated from in-trap fluorescence intensity f_n experimentally obtained with the fluorescence imaging. This new target intensity $I_{\mathrm{t},n}^{(i+1)}$ and the previously obtained phase pattern $\varphi^{(i)}$ serve as the input for the GS algorithm, which generates a new phase pattern $\varphi^{(i+1)}$ for the next iteration. As in the previous section, we run the GS algorithm for only $n_{\mathrm{GS}}=1$ cycle per iteration. We determine the initial correction factor $a_n^{(0)}$ and the initial phase pattern $\varphi^{(0)}$ from the results of the optimization with trapping light intensities. At every iteration, the in-trap fluorescence intensities are determined from 1,000 fluorescence images, each of which is captured after 300 ms loading and 20 ms PGC phases.

Figure 5(d) shows the resulting histograms of the integrated signals for the 4×4 square array. After only five iterations, the signal distributions for zero and single atom are clearly separated at all sites. The variance of in-trap fluorescence intensities can be reduced from 28.4 % to 2.4 %. The variance of trap depths, estimated from Eq. (4), is decreased from 20.8 % to 1.7 %. By analysis of the overlap of the Gaussian fits at all 16 sites, we find a decrease in the maximal detection error ε from 5.2 % to 0.002 %. The atomic loss on site 12 [see Fig. 5(f)] is also decreased from 8.0 % to 0.3 %, with the latter limited by the trap lifetime. We found that the uniformity is deteriorated by drifts of the phase modulation levels of the SLM, and which is mainly caused from the thermal drifts. By stabilizing the thermal drift of the SLM within 0.1 °C, the degradation of the uniformity cannot be observed over three months.

We apply this method to the various arrays of microtraps as shown in Fig. 2. A summary of the results is shown in Table 2 which indicates the structure of arrays, the number of traps N, the variance of in-trap fluorescence intensities σ_{fluo}, the variance of trap depths σ_{trap}, the maximal detection error ε, and the number of iterations required i. The method reduce σ_{fluo} to less than 6 % for all arrays within 10 iterations, while the convergence speed depends on the geometry and the number of sites. Without the optimization by taking in-trap fluorescence intensities, arrays have σ_{trap} between 9.1 % and 20.8 %. By applying this method, σ_{trap} is decreased to between 1.7 % and 4.0 %. Additionally, it is possible to realize high-fidelity detection

#259744 Received 25 Feb 2016; revised 30 Mar 2016; accepted 30 Mar 2016; published 6 Apr 2016

of individual single atoms in arrays containing up to 62 sites. The maximal detection error can be reduced to less than 10^{-4} for all arrays.

5. Conclusion

We have demonstrated the iterative feedback optimizations to realize highly uniformity of trap depths with the measurements of light intensities and in-trap fluorescence intensities emitted from single atoms. The feedback with in-trap fluorescence intensities reduce the variance of actual trap depths to 1.7 % for 4×4 square arrays and less than 4 % for all various arrays with up to 62 sites. We also observed a decrease in the detection error of single atoms. The error can be reduced to less than 10^{-4} for all arrays examined in this paper. It is possible to keep the detection fidelity of individual atoms in arrays up to 62 sites as almost same fidelity with typical single or two qubit experiments.

Recently, several experiments [10, 21] demonstrated ~ 90 % preparation efficiency of single atoms in a single and a few traps by using blue-detuned light assisted collisions, which require to carefully optimize the detuning of a homogeneous collision beam from the trap-shifted transition for each of all sites. Our method would help for their implementation on holographic arrays due to the variance of light shifts could be reduced.

Several experiments [22, 23] demonstrated blue-detuned traps, confining the atoms at the intensity minima, which reduces the light shifts on the atomic transitions. To the contrary, light shifts induced by red-detuned traps should be further precisely optimized for state control. In future work, further improvements for the precise optimization of the variance of light shifts could be achieved by the iterative feedback with the measurement of light shift spectra [24] of trapped single atoms. It is an important issue for coherent manipulation of trapped single atoms that different phases induced by the variance of light shifts across an array are accumulated and result in dephasing. A feedback system such as the one presented in this paper with holographic trap characteristics obtained by using in-trap atoms is useful for creation of finely optimized microtrap arrays.

Acknowledgments

This work was supported by Japan Society for the promotion of Science (Grants No. 24340095) and partly supported by research grant from Matsuo Academic Foundation.

#259744 Received 25 Feb 2016; revised 30 Mar 2016; accepted 30 Mar 2016; published 6 Apr 2016